Supplementary Information

Mechanism-Guided Discovery of a Blue-Light Receptor Clade

Lukas Ott[1], Américo T. Ranzani[1], Marius Blackholm[1], Annabelle Kamitz[2], Christian Renzl[2,3], Ole Bundgaard[4], Chongyao Wei[5], Andrés García de Fuentes[1], Tom Krebel[1], Carlo Unverzagt[4], Igor Schapiro[5], Günter Mayer[2,3], Andreas Möglich[1,6,7]

[1] Department of Biochemistry, University of Bayreuth, 95447 Bayreuth, Germany.
[2] Life and Medical Sciences (LIMES), University of Bonn, 53121 Bonn, Germany.
[3] Center of Aptamer Research & Development, University of Bonn, 53121 Bonn, Germany.
[4] Bioorganic Chemistry, Department of Chemistry, University of Bayreuth, 95447 Bayreuth, Germany.
[5] Theoretical Biophysics, University of Dortmund, 44227 Dortmund, Germany.
[6] Bayreuth Center for Biochemistry & Molecular Biology, Universität Bayreuth, 95447 Bayreuth, Germany.
[7] North-Bavarian NMR Center, Universität Bayreuth, 95447 Bayreuth, Germany.

Supplementary Tables

Supplementary Table 1 – Calculated (average isotopes) and observed mass peaks for unmodified *As*LOV2 C450A:F494M before and after irradiation as shown in Supplementary Figures 7a, b.

Species	Calculated *m*/*z*	Observed *m*/*z*	
		before illumination	after illumination
$[M+10H]^{10+}$	1,679.30	1,679.49	1,679.49
$[M+11H]^{11+}$	1,526.73	1,526.70	1,526.97
$[M+12H]^{12+}$	1,399.59	1,399.80	1,399.76
$[M+13H]^{13+}$	1,292.00	1,292.08	1,292.20
$[M+14H]^{14+}$	1,199.79	1,199.88	1,199.86
$[M+15H]^{15+}$	1,119.87	1,120.01	1,120.01
$[M+16H]^{16+}$	1,049.94	1,049.98	1,050.07
$[M+17H]^{17+}$	988.24	988.33	988.57
$[M+18H]^{18+}$	933.39	933.44	933.51

Supplementary Table 2 – Calculated (average isotopes) and observed mass peaks for the stable photoadduct between *As*LOV2 C450A:F494M and its flavin mononucleotide cofactor as shown in Supplementary Figure 7b.

Species	Calculated *m*/*z*	Observed *m*/*z*
$[M+10H]^{10+}$	1,724.94	1,725.04
$[M+11H]^{11+}$	1,568.22	1,568.38
$[M+12H]^{12+}$	1,437.62	1,437.81
$[M+13H]^{13+}$	1,327.11	1,327.20
$[M+14H]^{14+}$	1,232.38	1,232.55
$[M+15H]^{15+}$	1,150.29	1,150.41
$[M+16H]^{16+}$	1,078.46	1,078.62
$[M+17H]^{17+}$	1,015.08	1,015.25
$[M+18H]^{18+}$	958.74	958.89

Supplementary Table 3 – X-ray data collection and refinement statistics for *As*LOV2 C450A:F494M in its dark-adapted and pseudo-light-adapted states.

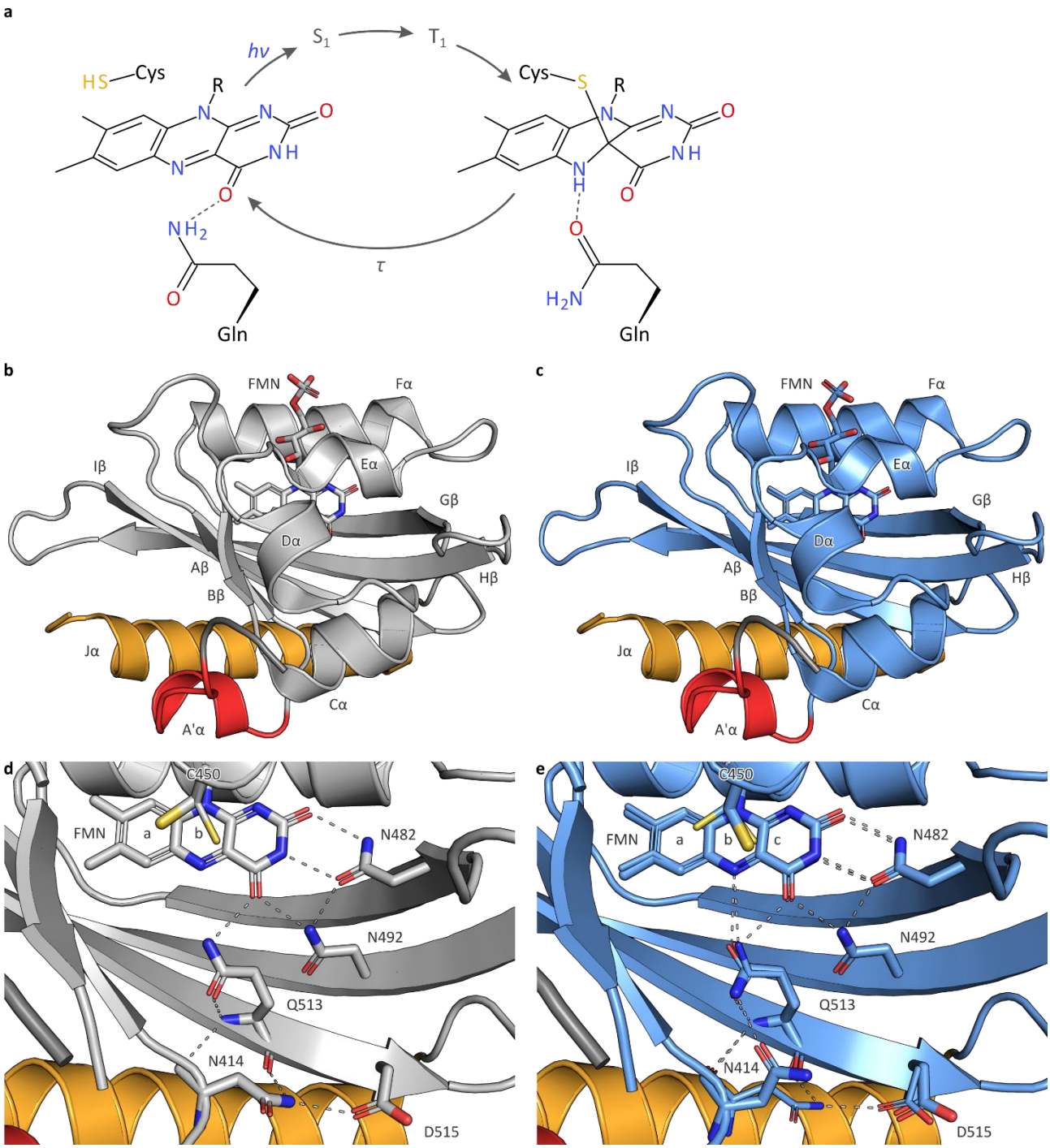
	***As*LOV2 C450A:F494M Dark Structure**	***As*LOV2 C450A:F494M Pseudo-Light Structure**
Data collection		
Space group	P2(1)2(1)2(1)	P2(1)2(1)2(1)
Cell dimensions		
a, b, c (Å)	35.08, 56.48, 67.11	35.65, 56.42, 66.58
α, β, γ (°)	90.0, 90.0, 90.0	90.0, 90.0, 90.0
Resolution (Å)	43.21 – 1.09 (1.16 – 1.09)	43.04 – 1.06 (1.12 – 1.06)
No. of reflections	393,666 (60,299)	435,740 (67,432)
No. of uniques	56,401 (9,006)	61,520 (9,775)
R_{meas} (%)	8.4 (149.8)	4.9 (163.7)
I / σ_I	11.97 (1.23)	17.13 (1.08)
Completeness (%)	100.0 (99.9)	99.8 (99.6)
Redundancy	6.98 (6.7)	7.08 (6.9)
B (Wilson) [Å^2]	15.12	16.24
Mosaicity [°]	0.086	0.105
$CC_{1/2}$	99.9 (52.1)	100 (52.2)
Refinement		
Resolution (Å)	43.21 – 1.09 (1.12 – 1.09)	43.04 – 1.06 (1.09 – 1.06)
No. reflections	54,306 (3,959)	59,446 (4,297)
R_{work} / R_{free}	0.132 / 0.157 (0.290 / 0.303)	0.137 / 0.172 (0.346 / 0.349)
No. atoms	1,833	1,990

Protein	1,537	1,664
Ligand/ion	40	112
Water	256	214
B-factors (Å^2)		
Protein	13.62	15.93
Ligand/ion	12.60	15.17
Water	29.99	34.27
R.m.s. deviation		
Bond length (Å)	0.010	0.011
Bond angles (°)	1.860	1.934
PDB deposition	pdb_000033sp	pdb_000033sq

26

Supplementary Figures

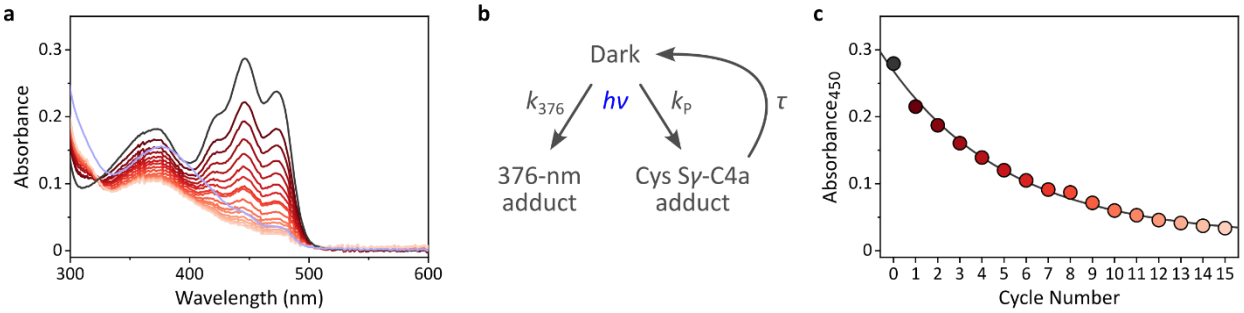
Supplementary Figure 1



Photocycle and three-dimensional structure of the light-oxygen-voltage (LOV) 2 domain from *Avena sativa* phototropin 1 (*As*LOV2). **a**, In the absence of light, *As*LOV2 non-covalently binds a flavin-mononucleotide (FMN) chromophore in its oxidized quinone state. Blue light excites the FMN cofactor to higher electronic singlet and vibronic states that rapidly converge onto the lowest vibronic level of the S_1 state (Kasha's rule). Following intersystem-crossing to the T_1 state on the nanoseconds

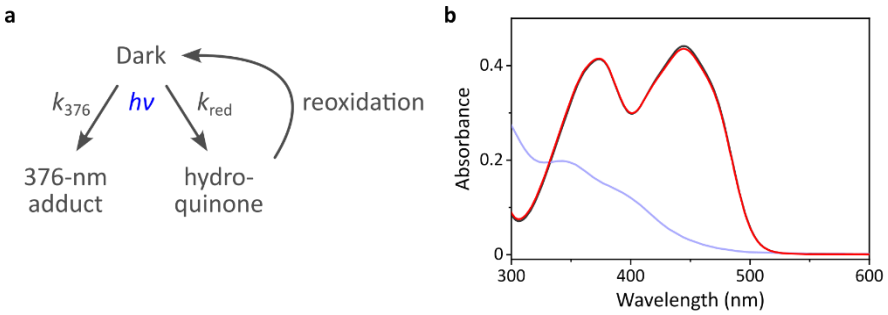
timescale, a covalent thioadduct forms between the Sγ atom of a conserved, proximal cysteine and the flavin C4a atom, likely via a radical-pair mechanism. The concomitant protonation of the flavin N5 atom is read out by a conserved glutamine residue that undergoes hydrogen-bonding rearrangements in response. The Sγ-C4a cysteinyl-flavin photoadduct is metastable and spontaneously ruptures in the thermal dark-recovery reaction. **b**, Three-dimensional structure of *As*LOV2 in its dark-adapted state as determined by X-ray crystallography (pdb 7pgx, [18]). α helices and β strands are labeled; the N-terminal and C-terminal A'α and Jα helices that underlie blue-light-dependent signal transduction are highlighted in orange and red. **c**, Three-dimensional structure of *As*LOV2 in its pseudo-light state captured by freeze-trapping crystallography (pdb 7pgy, [18]). **d**, Chromophore-binding pocket of dark-adapted *As*LOV2 with key residues engaged in FMN contacts and signal transduction marked. **e**, Chromophore-binding pocket of pseudo-light-adapted *As*LOV2. The active-site cysteine 450 rearranges compared to the dark-adapted structure, but owing to X-ray-induced photolysis, no covalent bond is observed to the flavin C4a atom [15,18]. As a hallmark of downstream signal transduction, residue N414 exhibits a rearrangement of its amide sidechain. Alternate conformations of residues in panels d and e are denoted by lower-case letters.

Supplementary Figure 2



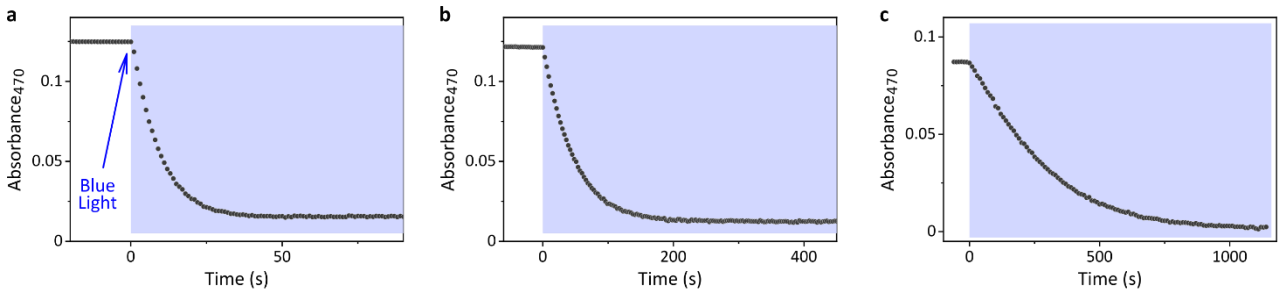
Competing photochemical reactions in the F494M variant of *Avena sativa* phototropin 1 LOV2 (*As*LOV2). **a**, UV-vis absorbance spectra recorded for *As*LOV2 F494M in its dark-adapted state (black line) and after blue-light exposure (blue line). From top to bottom, the red curves denote spectra acquired after iterative cycles of blue-light exposure and subsequent dark recovery. **b**, Reaction scheme used for analyzing the data in panel a. Starting from its dark-adapted state, the F494M variant can either form the canonical cysteinyl-flavin Sγ-C4a photoadduct (right branch, rate constant k_P) or the 376-nm photoadduct (rate constant k_{376}). Whereas the canonical photoadduct eventually recovers to the original dark-adapted state, the 376-nm photoadduct does not. Thus, the fraction of molecules undergoing the canonical photochemistry successively drops with increasing illumination cycle number, as experimentally observed in panel a. **c**, Absorbance at 450 nm within the spectra after dark recovery as a function of illumination cycle number (see panel a). Evaluation of these data (solid line) determined a k_{376}/k_P ratio of 0.20.

Supplementary Figure 3



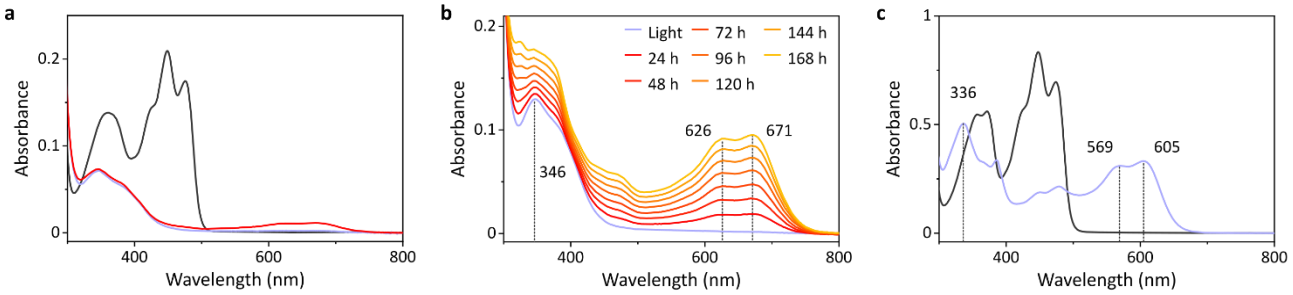
Competing photochemical reactions in the C450A:F494M variant of *Avena sativa* phototropin 1 LOV2 (*As*LOV2). **a**, Starting from its dark-adapted quinone state, the CA:FM variant predominantly forms the irreversible 376-nm photoadduct with rate constant k_{376}. A minor proportion, however, instead undergoes photoreduction to the fully reduced hydroquinone that slowly reoxidizes to the quinone. **b**, Reversible photoreduction of the flavin quinone to the hydroquinone state. UV-vis absorbance spectra of free flavin mononucleotide were acquired in the presence of 20 mM EDTA before illumination (black line), after saturating exposure to blue light (470 nm, blue), and upon ensuing recovery in darkness (red).

Supplementary Figure 4



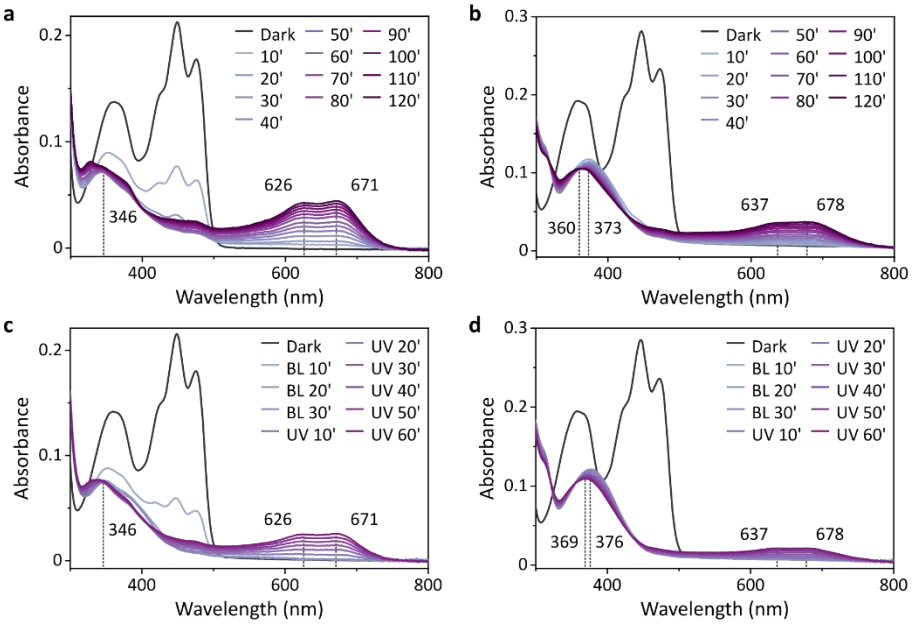
Kinetics of photoadduct formation in *Avena sativa* phototropin 1 LOV2 (*As*LOV2) wild type vs. the C450A:F494M and C450M variants. **a**, Wild-type *As*LOV2 within its dark-adapted state was incubated at 22°C before exposure to constant blue light (470 nm, 2 mW cm^{-2}). The resultant formation kinetics of the cysteinyl-flavin Sγ-C4a photoadduct were tracked by absorbance at 470 nm and fitted to a single-exponential function with rate constant of (0.112 ± 0.001) s^{-1}. **b**, Using the same illumination intensity and geometry as in panel a, the 376-nm photoadduct of the *As*LOV2 CA:FM variant formed in a single-exponential fashion with a rate constant of (2.19 ± 0.01) × 10^{-2} s^{-1}. **c**, Again under the same illumination conditions, the C450M variant adopted its 346-nm state with single-exponential kinetics with a rate constant of (3.44 ± 0.01) × 10^{-3} s^{-1}.

Supplementary Figure 5



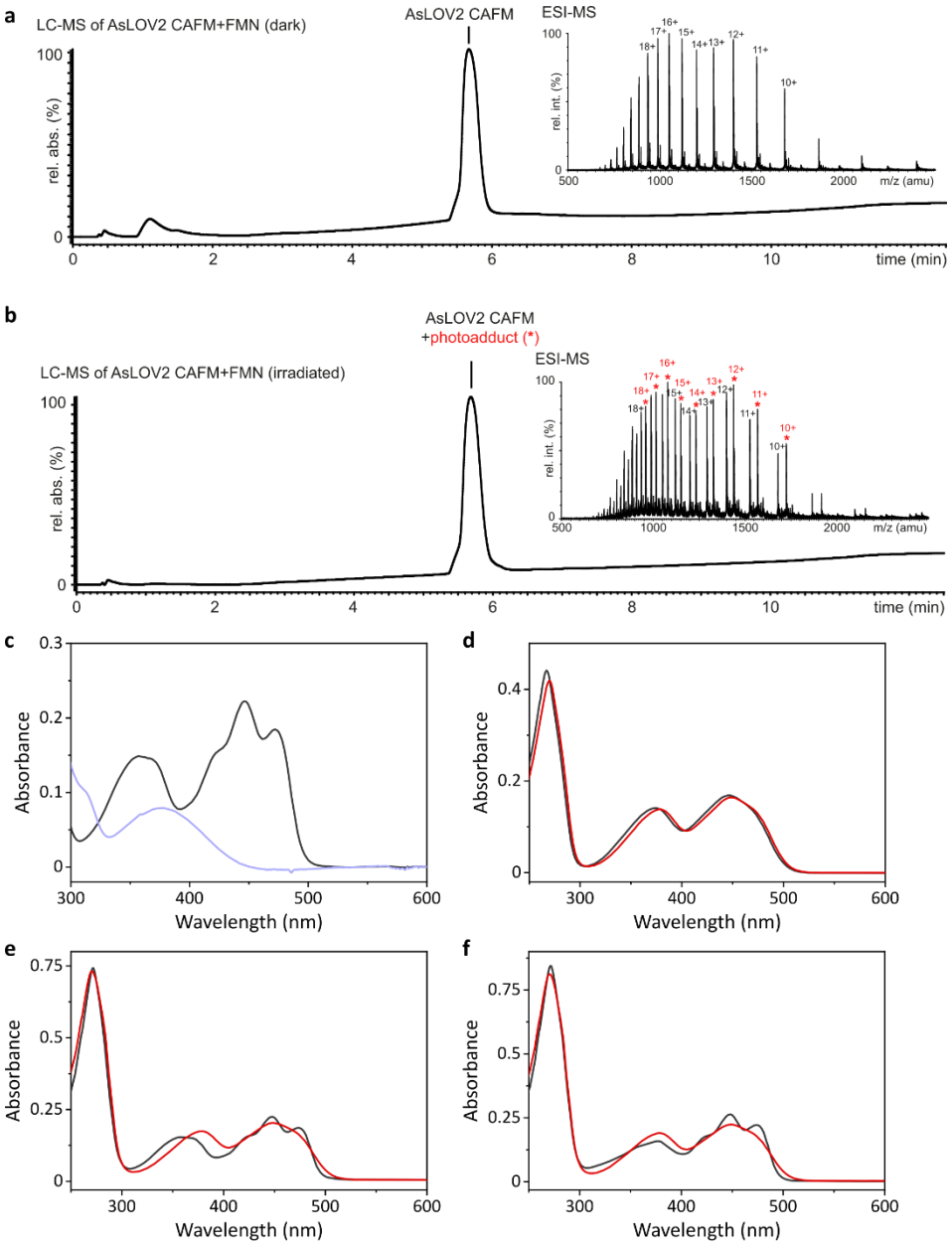
Spectroscopic investigation of the *Avena sativa* phototropin 1 LOV2 (*As*LOV2) variants C450M and C450A. **a**, UV-vis absorbance spectra of *As*LOV2 C450M acquired for the dark-adapted sample (black line), upon blue-light exposure (blue), and after subsequent recovery in darkness at 22°C (red). **b**, After initial blue-light irradiation (blue line), the dark recovery reaction of *As*LOV2 C450M was monitored over several days at 22°C (red to orange lines). The absorbance maxima of the initially formed 346-nm photoproduct and the state it gradually evolves into are marked. **c**, UV-vis absorbance spectra of *As*LOV2 C450A for the dark-adapted sample (black line) and upon saturating blue-light exposure in the presence of the reductant TCEP.

Supplementary Figure 6



Response of the *Avena sativa* phototropin 1 LOV2 (*As*LOV2) variants C450M and C4504:F494M to UV irradiation. **a**, UV-vis absorbance spectra of *As*LOV2 C450M acquired for the dark-adapted sample (black line) and following exposure to ultra-violet light (390 nm, 10 mW cm^{-2}) for up to 120 min (blue to violet lines). **b**, As panel a but for the CA:FM variant. **c**, Following acquisition of a spectrum of the dark-adapted sample (black), *As*LOV2 C450M was first irradiated with blue light (BL, 470 nm, 2 mW cm^{-2}) for 30 min and then with UV light (UV, 390 nm, 10 mW cm^{-2}) for another 60 min. **d**, As panel c but for the CA:FM variant.

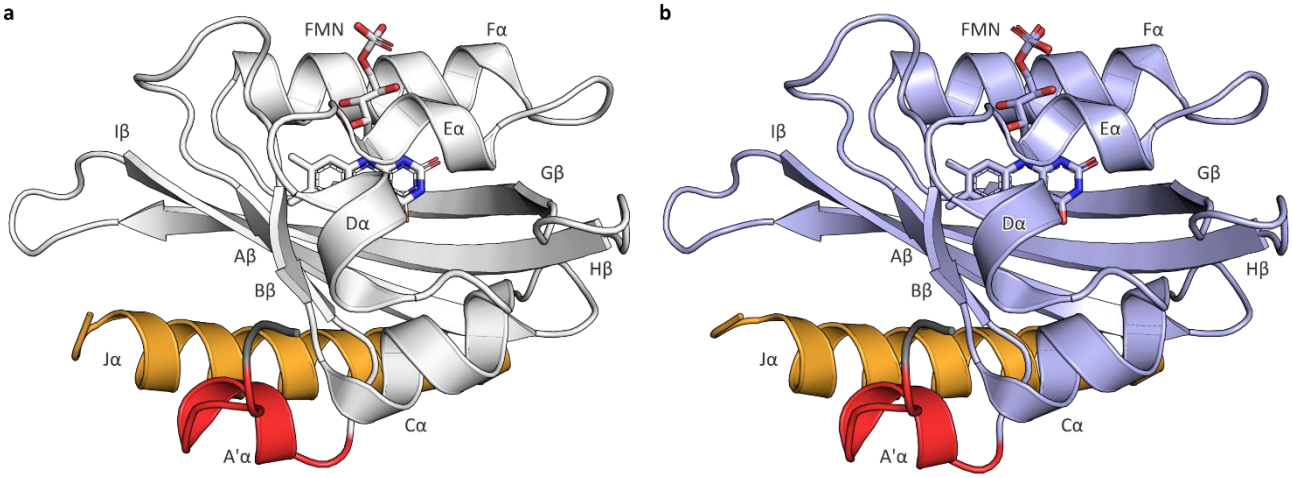
Supplementary Figure 7



Mass-spectrometric analysis of the 376-nm photoadduct in *Avena sativa* phototropin 1 LOV2 (*As*LOV2) C450A:F494M. **a**, Dark-adapted *As*LOV2 CA:FM was incubated in darkness at 22°C for 20 min, diluted into 0.1% formic acid, and analyzed by reverse-phase ultra-performance liquid chromatography (UPLC) on a C5 column. The electrospray ionization mass spectrum of the peak eluting at 5.8 min is shown as the inset. The mass species calculated for the *As*LOV2 CA:FM protein and the observed values are provided in Suppl. Table 1. **b**, Procedure as in panel a, but the initial 20-min incubation took place under constant 450-nm light (2 mW cm^{-2}) rather than in darkness. The mass spectrum of the main elution peak reveals signals corresponding to the original protein (marked

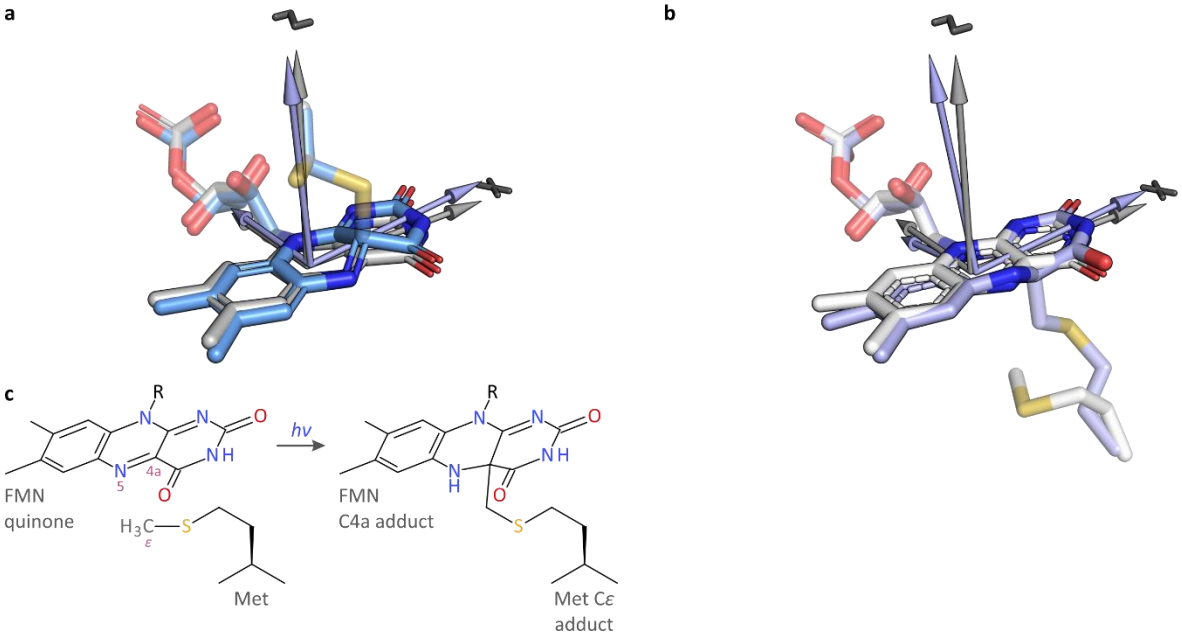
in black) and an additional species (red). Calculated and observed mass peaks of the unmodified and modified species are given in Suppl. Tables 1 and 2, respectively. The presence of the original mass signal of the apo-protein after illumination can be attributed to incomplete flavin loading, estimated to be around 70% based on absorbance measurements (see panels c-f). **c**, UV/vis absorbance spectra of the dark-adapted (black line) and blue-light-irradiated *As*LOV2 CA:FM samples (blue line) used for the chromatographic and mass-spectrometric analyses shown in panels a and b. **d**, UV/vis absorbance spectra of flavin mononucleotide in native buffer (black line) and 5 M guanidinium chloride (red line). **e**, UV/vis absorbance spectra of dark-adapted *As*LOV2 CA:FM in native buffer (black line) and 5 M guanidinium chloride (red line). **f**, As panel e but for wild-type *As*LOV2.

Supplementary Figure 8



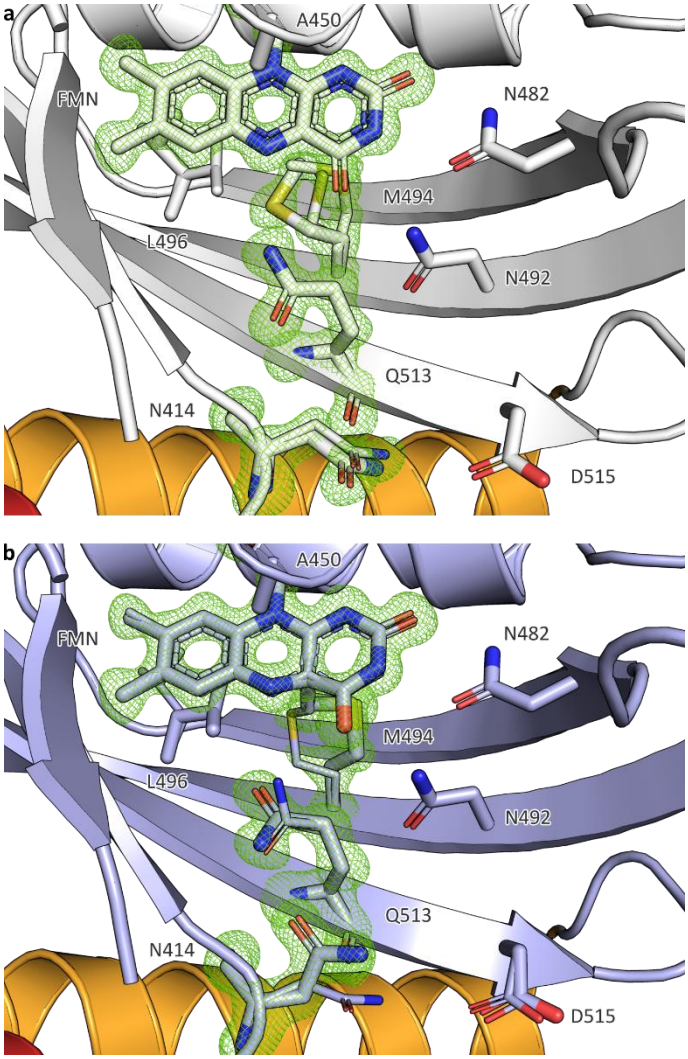
Three-dimensional structures of *Avena sativa* phototropin 1 LOV2 (*As*LOV2) C450A:F494M. **a**, Structure of the dark-adapted state in the same orientation as the wild-type protein in Suppl. Fig. 1b. The FMN cofactor is shown in stick representation and is labeled, as are the α-helices, and the β-strands. **b**, Structure of the pseudo-light state determined by freeze-trapping crystallography.

Supplementary Figure 9



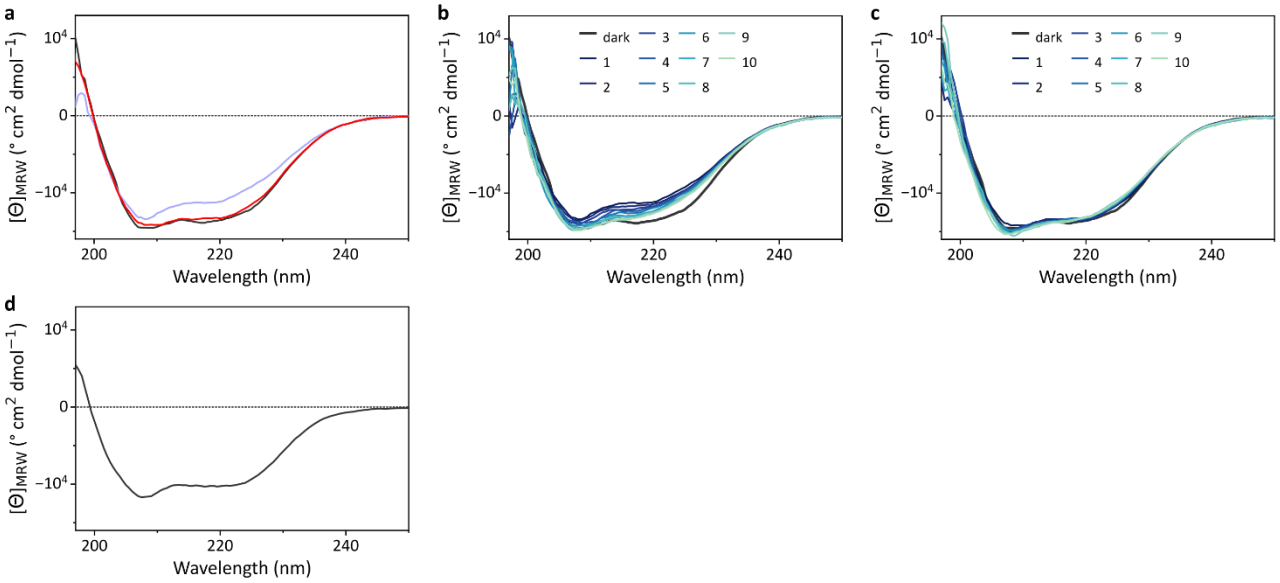
Reorientation of the flavin-mononucleotide (FMN) chromophore in *Avena sativa* phototropin 1 LOV2 (*As*LOV2) wild type vs. C450A:F494M upon formation of the respective photoadduct. **a**, To evaluate the chromophore movement upon formation of the canonical cysteinyl-flavin Sγ-C4a adduct, the three-dimensional structures of *As*LOV2 wild type in its dark-adapted (grey sticks, pdb entry 2v1a, [25]) and pseudo-light states (petrol sticks, pdb entry 2v1a, [25]) were superposed. The coordinate systems denote the principal axes of the flavin isoalloxazine in the two structures with the *z*-axis normal to the aromatic ring plane. Upon Sγ-C4a photoadduct formation, the isoalloxazine tilts by around 5.3° and 2.7° along the *x*- and *y*-axes, respectively. **b**, As in panel a but for *As*LOV2 CA:FM based on the crystal structures solved at present. Formation of the methionyl-flavin Cε-C4a photoadduct entails tilting of the isoalloxazine plane by around 4.2° and –7.7° along the *x*- and *y*-axes, respectively. For clarity, panels a and b only show the major conformations of the adduct-forming residues and the flavin cofactor. **c**, Lewis structure of the methionyl-flavin Cε-C4a photoadduct in the *As*LOV2 CA:FM variant.

Supplementary Figure 10



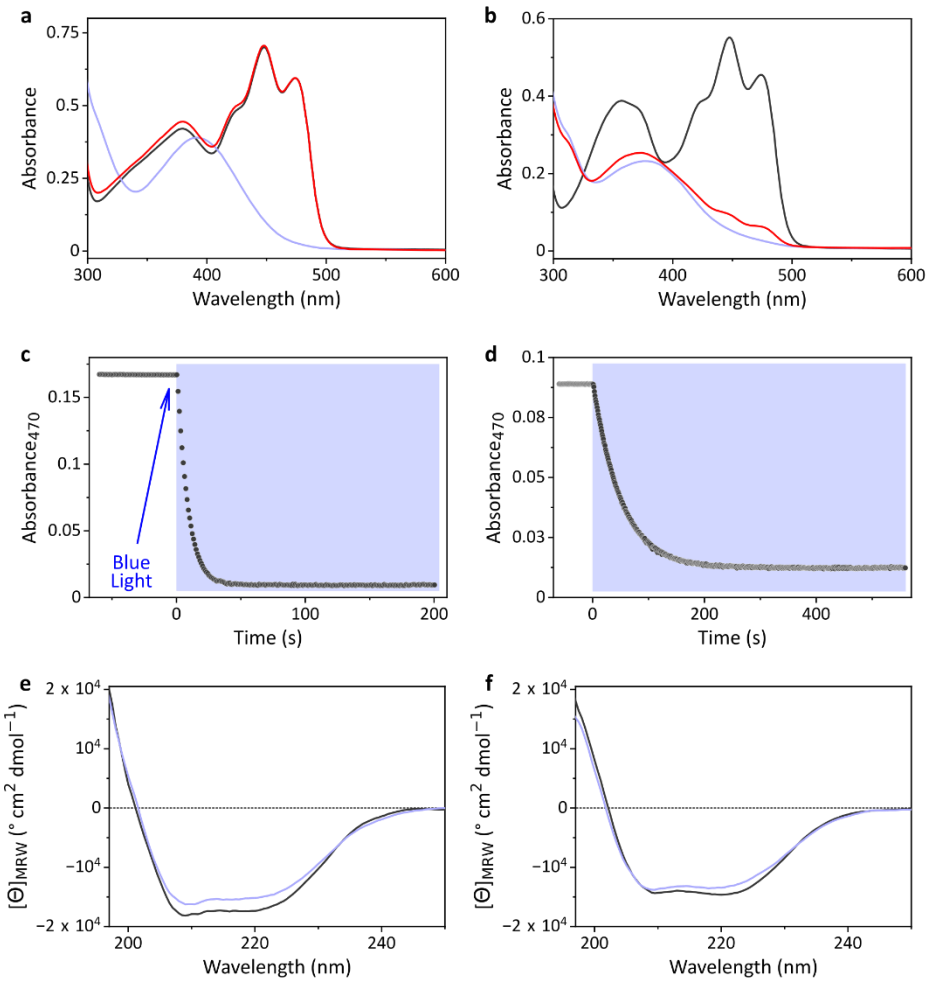
Signal transduction in the *Avena sativa* phototropin 1 LOV2 (*As*LOV2) C450A:F494M variant. **a**, Residues involved in signal transduction within dark-adapted *As*LOV2 CA:FM. For better visibility, the helices Cα and Dα are omitted from the display. The green mesh denotes a *Fo-Fc* omit electron density map contoured at +3.0 σ. **b**, As panel a but for the pseudo-light structure of *As*LOV2 CA:FM.

Supplementary Figure 11



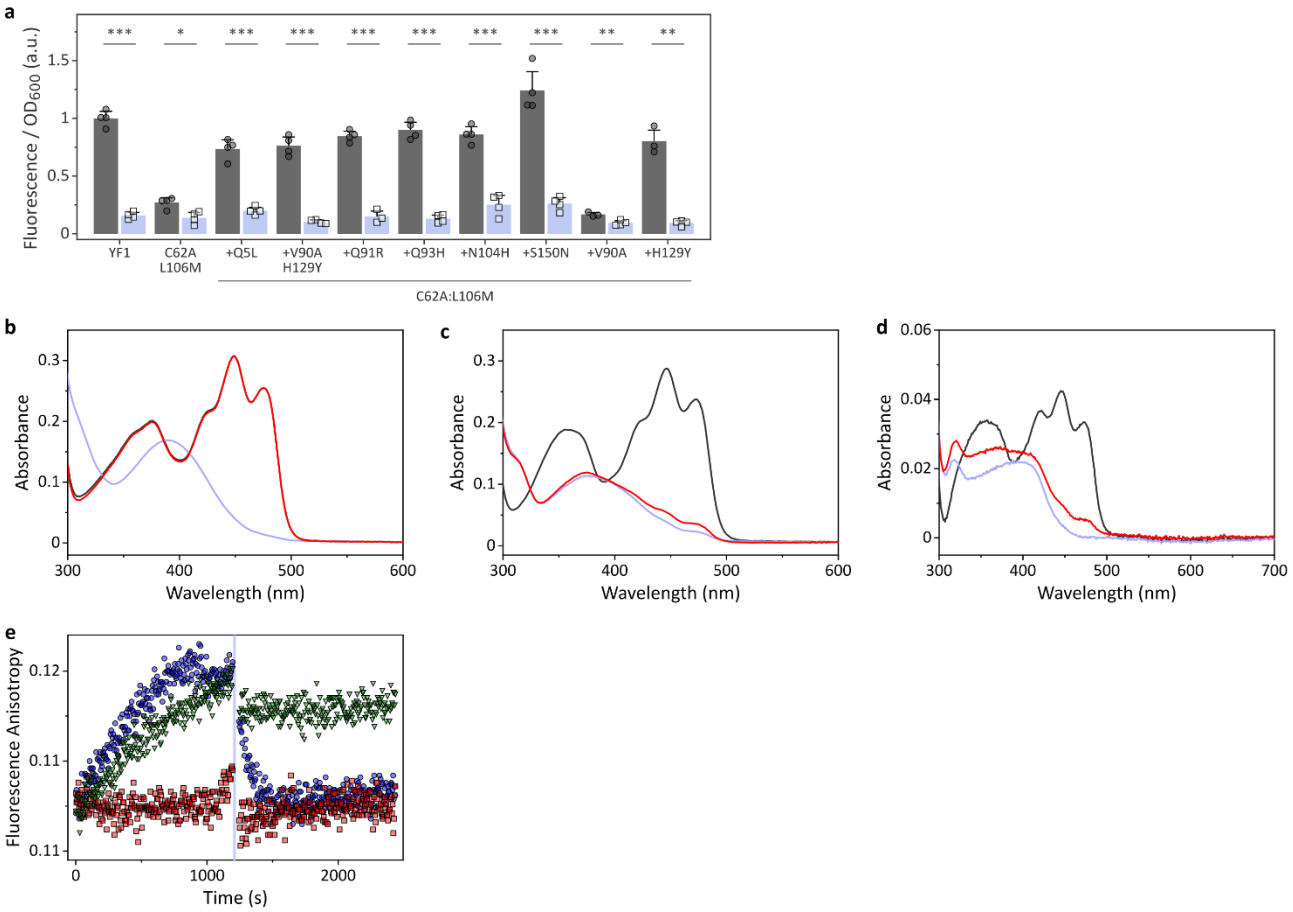
Structural response of the *Avena sativa* phototropin 1 LOV2 (*As*LOV2) F494M variant to repeat blue-light exposure. **a**, Far-UV circular dichroism spectra of *As*LOV2 F494M in the dark-adapted state (black line), immediately upon exposure to blue light (blue line), and after recovery in darkness (red line). **b**, As panel a but the sample was subjected to iterative cycles of blue-light exposure and ensuing dark recovery. The colored lines show CD spectra immediately after a given illumination event (indicated by numbers). **c**, Likewise, far-UV spectra were recorded for each iterative cycle after 30 min of dark recovery. Individual cycles are color-coded and labeled as in panel b. **d**, Far-UV CD spectrum of the *As*LOV2 C450A variant in its dark-adapted state.

Supplementary Figure 12



Spectroscopic characterization of the iLID [26] *As*LOV2 derivative. **a**, UV-vis absorbance spectra of iLID bearing the V416L exchange recorded in the dark-adapted state (black line), after blue-light exposure (blue), and upon ensuing recovery in darkness (red). Notably, the V416L exchange slows down the dark-recovery reaction and thereby renders the protein effectively more light-sensitive at photostationary state. **b**, Corresponding spectra for iLID V416L:C450A:F494M. **c**, The kinetics of cysteinyl-flavin Sγ-C4a photoadduct formation in iLID V416L upon exposure to constant blue light (470 nm, 2 mW cm^{-2}) were monitored by absorbance at 470 nm. The time course can be described by a single-exponential function with a rate constant of (0.119 ± 0.001) s^{-1}. **d**, As panel c but for the blue-light-induced formation of the methionyl-flavin Sε-C4a photoadduct. A single-exponential fit of the absorbance data yielded a rate constant of (2.02 ± 0.01) × 10^{-2} s^{-1}. **e**, Far-UV circular dichroism spectra of iLID V416L prior to (black line) and after exposure to blue light (blue line). **f**, As panel e but for iLID V416L:C450A:F494M.

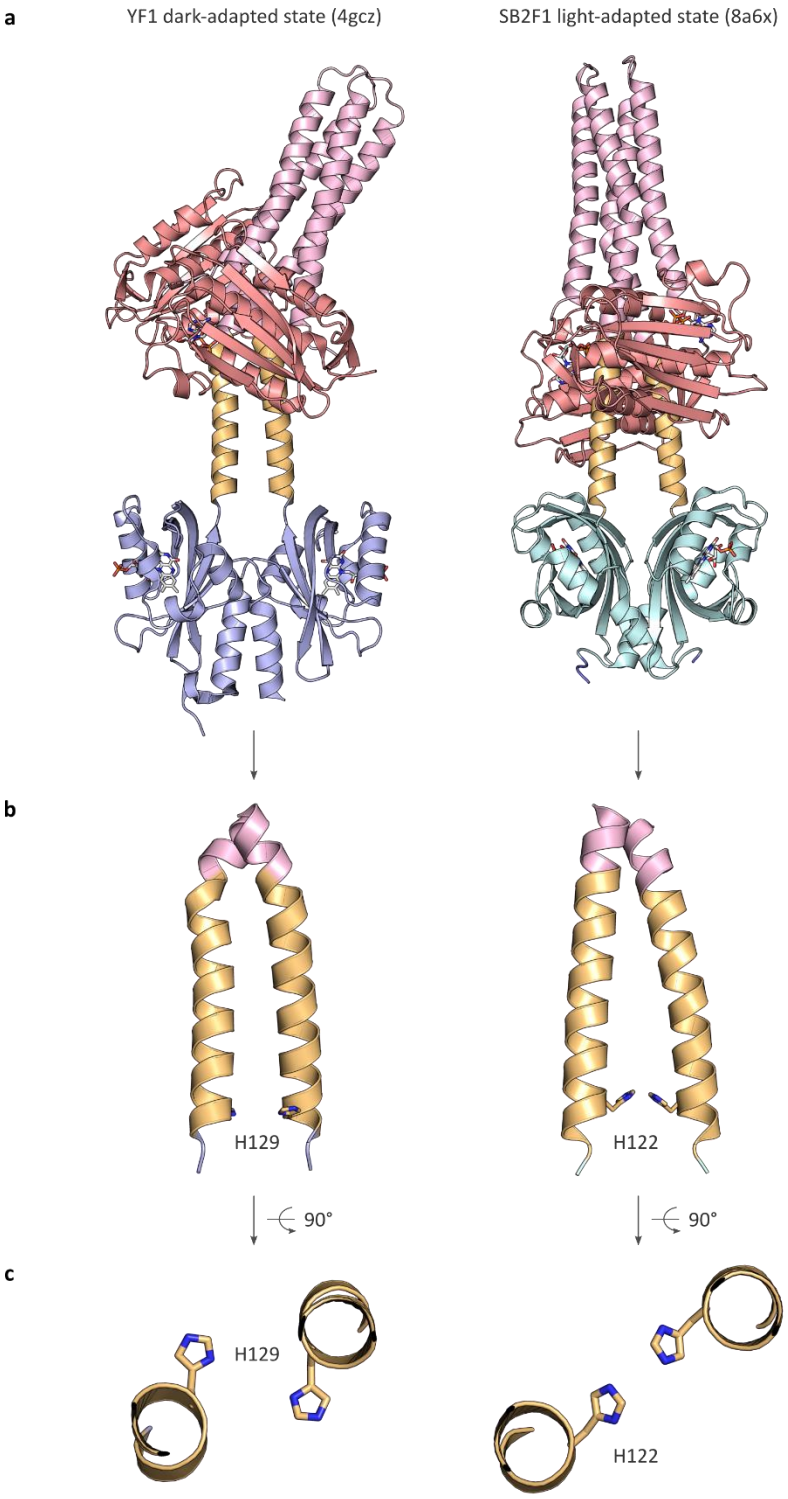
Supplementary Figure 13



Spectroscopic and functional characterization of variants of the engineered LOV-histidine kinase YF1. **a**, Analysis of variants identified by random mutagenesis in the YF1 C62A:L106M background. *Escherichia coli* bacteria harboring a pDusk-*Ds*Red plasmid encoding a given YF1 variant were incubated in darkness or blue light, followed by measurements of reporter fluorescence and optical density at 600 nm (OD_{600}) of the bacterial culture. Fluorescence data were divided by OD_{600} and normalized to the reference value observed for the original YF1 when incubated in darkness. Data represent mean ± s.d. of 4 biological replicates, individually shown as circles and squares. Symbols above the bars denote results from Welch's two-sided *t*-tests for the pairwise comparison of dark vs. light conditions (n.s. not significant, * $p < 0.05$, ** $p < 0.01$, *** $p < 0.001$). **b**, UV-vis absorbance spectra of YF1 in its dark-adapted state (black line), after blue-light exposure (blue), and upon subsequent recovery in darkness (red). **c**, As panel b but for the YF1 variant C62A:L106M. **d**, As panel b but for the YF1 variant C62A:L106M:H129Y. **e**, The activity and light response of YF1 (blue circles) and its C62A:L106M (red squares) and C62A:L106M:H129Y (green triangles) variants were

assessed in a coupled fluorescence anisotropy assay [18]. Briefly, a given, dark-adapted YF1 variant was incubated in the presence of its cognate response regulator FixJ and a fluorescently labeled, double-stranded DNA substrate, labeled at its end with a tetramethylamino-rhodamine (TAMRA) fluorophore and comprising the FixK2 operator sequence. Addition of ATP at time zero allows FixJ phosphorylation by the YF1 variant. Once phosphorylated, FixJ homodimerizes and binds the FixK2 epitope. The resultant slowdown of rotational tumbling of the DNA substrate leads to a higher TAMRA fluorescence anisotropy which is tracked over time. At around 1,200 s (indicated by the blue bar), the samples were illuminated with intense 470-nm light for 30 s before the measurement then continued for another 1,200 s.

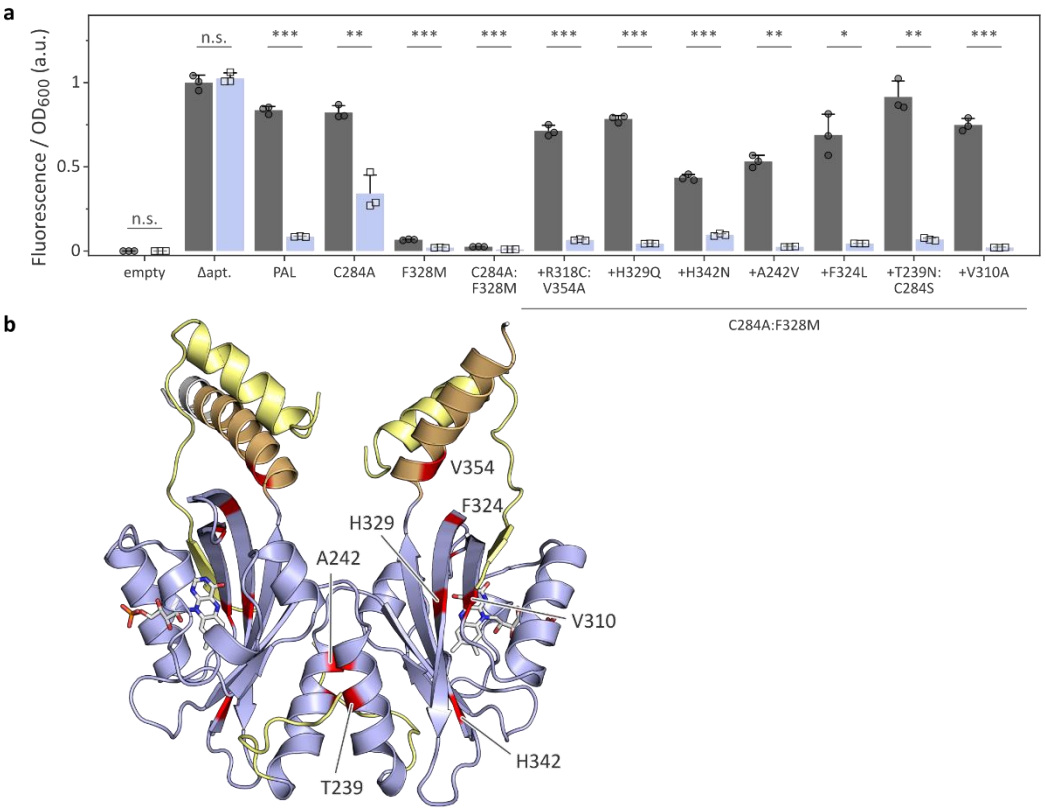
Supplementary Figure 14



Location of histidine 129 within the YF1 histidine kinase. **a**, Structural alignment of YF1 (left, pdb 4gcz [30]) and the YF1 derivative SB2F1 (right, 8a6x [32]). Whereas the YF1 structure represents the dark-adapted receptor state, that of SB2F1 is assumed to correspond to the light-adapted conformation [32]. The Jα helical linker connecting the LOV photosensor dimer and the histidine-kinase DHp/CA

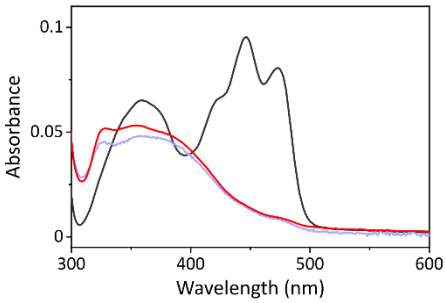
effector module is instrumental in signal transduction and is highlighted in orange. **b**, The close-up view of the Jα linkers in YF1 (left) and SB2F1 (right) shows the location of histidine 129 within both structures. Note that residue 129 of YF1 corresponds to residue 122 in SB2F1. **c**, Within the YF1 structure (representative of the dark-adapted state), the Jα helices assemble into a parallel homodimeric coiled coil with H129 in its '*a*' register. By contrast, within SB2F1 (emblematic of the light-adapted state), the Jα helices are displaced and rotated by around 50° [32]. Replacement of H129 by a bulkier tyrosine residue might hinder adoption of the conformation seen in the SB2F1 structure and thereby favor the dark-adapted, kinase-active state evidenced in the YF1 structure.

Supplementary Figure 15



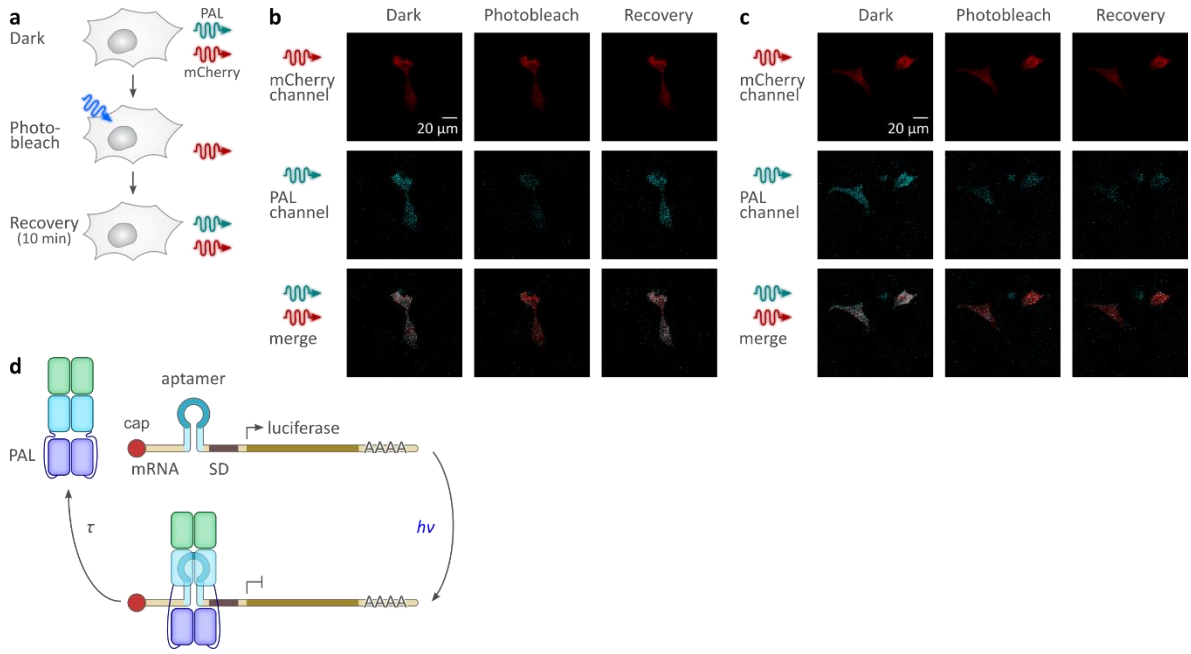
Screening for variants restoring blue-light-dependent signal transduction in the PAL context. **a**, The LOV moiety of the PAL C284A:F328M variant was subjected to random mutagenesis, and potential effects on signal transduction were assessed in the pCrepusculo-*Ds*Red reporter background (see Fig. 4a-b). Whereas PAL CA:FM elicited only weak blue-light responses, several PAL variants bearing additional residue exchanges as indicated in the figure restored or even surpassed the light response afforded by wild-type PAL. Symbols above the bars denote results from Welch's two-sided *t*-tests for the pairwise comparison of dark vs. light conditions (n.s. not significant, * $p < 0.05$, ** $p < 0.01$, *** $p < 0.001$). **b**, The location of the residues exchanged in the PAL CA:FM variants with restored light response were plotted in red onto the three-dimensional structure of the homodimeric LOV moiety of dark-adapted PAL [33].

Supplementary Figure 16



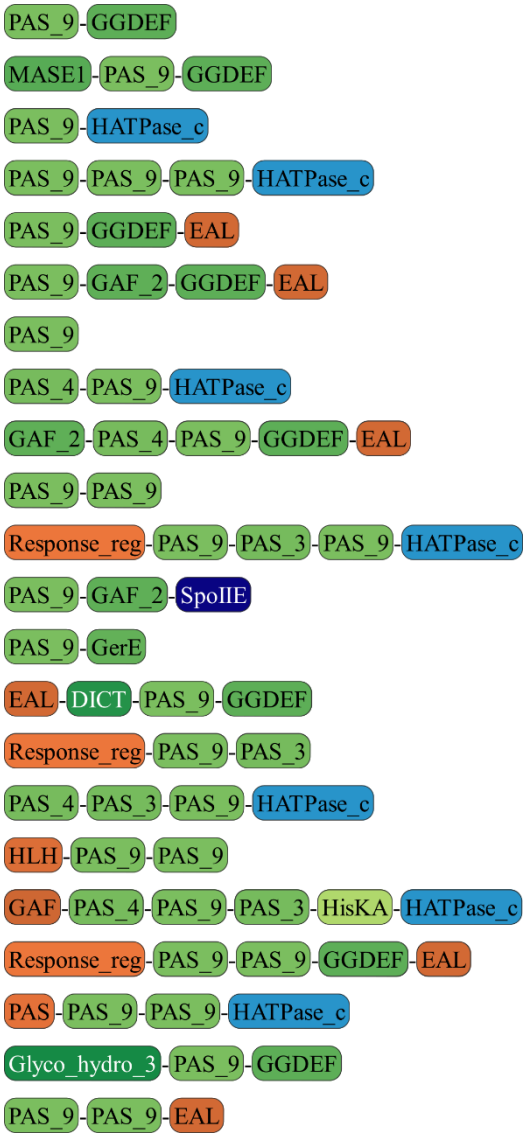
UV-vis absorbance spectra of PAL C205A:C284A:V310A:F328M in its dark-adapted state (black line), after blue-light exposure (blue), and upon subsequent recovery in darkness (red).

Supplementary Figure 17



Optoribogenetics with PAL variants in mammalian cells. **a**, Wild-type PAL and its LOVme variant (C284A:V310A:F328M) were fused with an N-terminal mCherry tag [33] and stably expressed in HeLa cells. The functional expression of the PAL variant and the mCherry tag can be ascertained by fluorescence microscopy in the green and red emission channels, respectively. Exposure to blue light, i.e., photobleaching, incurs photoactivation of PAL and adoption of its light-adapted photoadduct state which is less fluorescent. At least for wild-type PAL, this state forms reversibly and reverts to the original, dark-adapted state over time, thus eventually restoring the initial fluorescence signal. **b**, Fluorescence micrographs of HeLa cells expressing mCherry covalently linked to wild-type PAL. The individual columns show micrographs of the same field of view prior to light exposure, immediately upon photobleaching, and after 10 min recovery at 37°C. From top to bottom, the rows show micrographs in the green and red emission channels, and with both channels overlaid. The scale bar denotes 20 µm. **c**, As panel b but for the C284A:V310A:F328M variant. **d**, Setup for the optoribogenetic regulation of mammalian gene expression using PAL variants [33]. In its light-adapted state, PAL binds to a motif-3 aptamer embedded in the 5'-untranslated region of an mRNA and thereby lowers the expression of a luciferase reporter gene.

Supplementary Figure 18



A BLAST search against GenBank for LOV receptors lacking the active-site cysteine but bearing a methionine residue in the position corresponding to F494 in *Avena sativa* phototropin 1 LOV2 identified around 50 candidate receptors. These were analyzed concerning their domain architecture according to the Pfam classification [62]. The architectures observed across all the LOVme candidates are shown schematically. Identifiers for specific receptors are provided in Suppl. Fig. 19a. Note that LOV domains belong to the Pfam PAS superfamily; the LOVme modules are thus annotated as 'PAS_9' in the figure.

a



```
AsLOV2          404 LATTLERIEKNFVITDPRLPDNP---IIFASDSFLQLTEYSREEILGRNCRFLQGPETDRA---------TVRKIRDAIDNQTEVTVQLINYTKSGKKFWNLFHLQPMRDQKGDVQYFIGVQLDGTEH  519
AML78281.1      474 IASALRLIMRNIVVTDPKQSGNP---IIYCTQGACQMTQYGKDEILGRNGGFLQGAASDPV---------TKSQIGKALRESRECLAEMLNYKKDGLPFWNLMFITPVLDALGKPFLFIGVQYDITLR  589
AVM73519.1      347 SEQVLQTVSNGVAIADATQPDFP---LVYVNPAFESMTGYKAADVVGTNARFLHRDDYDQP---------DLARLRTALETGGSVHVVLRNYRADGSLFWNDMTVSAVHAITGGLTHFVAIQRDITEQ  462
WP_211546189.1  343 SERVLETVSNGVAISDATRPDFP---LVYVNPAFESMTGYSAAEVLGRNPRFLHGDDREQI---------GLVEVRKALKAGHSVDAVLKNYRADGTPYWNDMTISAVHAVSGHLTHFVAIQRDITEQ  458
WP_416816808.1  146 -----LSAAVNGVIITLAGGDMP---VVYVNPAIEHITGYPADEILGRNFRFLQNDDRQQP---------DIARVHEALARGDACRAVLRNYRKDGSLFWNRMSIWPVKDPQGQTTHFVGIQEDITEQ  256
MFO1469322.1     14 -----DTAPIGIAIVDATNPEHP---VVYANQEFCQLTGHALEEILGRNLRFLQGEDRDQD---------ARHRLRESLERGEPTRVLLRNYRKDGTLFWNEMSVVPLKDAAGFITHFAGFHRDAGER  124
MBS0612441.1     14 -----EAAPIGVVLVDATNPEHP---LVYANQEFCHLCGFAMNELLGRNLRFLQGEDREQD---------ARQRLRESLERGEAARVLLRNYRKDGSLFWNEMSVVPLKDAAGFITHFAGFHRDAGER  124
HXA37140.1        9 YRRLVESSPEGVLLVDARNPEHP---VIYANPGFEALTGYSAAELLGRNPRFLQADDREQD---------GRHRLREALGRGESCRVLLRNYRKDGSLFWNEMTVLPLLDADGRVTHFVGHHRDAGER  124
HEY4971561.1     14 ----VETSPEGVVLVDAQHPEHP---VIYANSGFEALTGYSSAQLLGRNLRFLQSEDREQD---------GRHRLREALGRGESCRVLLRNYRKDGTLFWNEMSVLPLLGADGRVTHFAGHHRDAGER  125
HEY1312879.1      9 YRRLVETSPEGVVVVDAQNPEQP---VIYANPGFEALTGYAAAELVGRNLRFLQADDREQD---------GRNRLREALGRGEPCRVLLRNYRKDGTVFWNEMTALPLRDAEGRITHFVGHHRDAGER  124
HXC10320.1       13 ----VDTSPEGVVLVDAQDPERP---VIYVNPGFEALTGYSAAELLGRNLRFLQGDDREQD---------GRQRLREALKVGESCRVLLRNYRKDGRVFWNEMTVLPLLDAGGRVTHFVGHHRDAGER  124
HXI76895.1        9 YRRLVETSPEGVAVVDALHPERP---AVYVNPGFEALTGYSAAELVGRNLRFLQADDREQD---------GRHRLREALKLGESCRVLLRNYRKDGRVFWNEMTILPLLDPQGRVTHYVGHHRDAGER  124
MDF3019588.1     32 ------------------GERA---AVYANPAFCRLTGYELSELIGKNLRFLQGDDRDQP---------ELDPIRESLRHGEPVRALLRNQRKDGTVFVNDMQLYPLKDGGGKVTHFIGYHREGGTR  128
HEX6638526.1     31 ------------------GGERK---VVYVNPAFCRLTGYELHELIGKNPRFLQADDREQP---------ELETVREALRHGEPVRALLRNSRKDGTVFVNDMQIYPLKDGDGKVTHFIGYHREGGTR  128
HVF16775.1        9 LKHLVESAPEGVALCEARGGDWP---VVFVNPALEQLTGYSADQIVGRNLRFLQADDRDQE---------GVLKIKNALRDGDPCHALIRNYRRDGTMFWNEMRLVPIRADDGQITHFASFHR-EGAT  123
MDZ7747625.1    127 IAAGADEPRRGLIIADAHSPDLP---IQYVDRIFCRIGGYSPGEVIGRNARFLQGDDRDQP---------GRWRLAGALRRGEPCTVVLRNYRRDGGLFENRMEVTPVFGVDE--------------  227
MDE2123407.1    207 LKAAIEASEFGVCVADAQTPDYP---LVYVNPGFERISGYTAAQALGRNPRFLQGGENKQP---------ALEELRAALREGRSCSVQLRNVRADGRVFWNEMSLAPVRDEGGTITHVVGLINDVS--  320
HEU0102320.1    397 --------SNGLCICDARLPDLP---MVYVNPAMERLTGYDADHLLGRNPRFLQGGVADPD---------AVAGISRQLRLGREARVTLRNRRPDGTPWWNEMHLLPVRDRSGTITNWVGTANDVTAR  504
HEV2742216.1     27 -------CANAVIITDAKLPDGP---VVYANPAAERITGYPLEEILGRNPRFLQGPYSDLE---------EVAKLRRAIAEGREFYGVLRNRRKDGSDFFNEMHVAPVRDGDGALTHFVGIQNDATER  135
CAA9447600.1     32 -------CANAVIITDAAQPDSP---AVYANPAAEHITGYPLEEILGRNPRFLQGPYSDLE---------EVAELRRAVAEGREFYGVVRNRRKDGSDFFNEMYVAPVRDGDGAVTHFVGIQNDVTER  140
MEA3044548.1     12 ------DSGIAFAITDPRRPDNP---LVAVNEAFSHLTGYEAGESIGRNPRFLQGPMSEEA---------ARAVVRHAVAAHQPAITEIWNYRRDGSAFRNAMMVAPVFGDDGELAFYLGSQVDVGLV  121
MDX2138964.1    402 -------TVGIVICSAQRADDYA---VLYANSAFEQITGYCQEEIIGRNLRFLQGADRNQP---------DLKILRHSLQTGSECAVTLRNYHKQGHLYWIEMWISPVFDTEGKLSHFIGIQYDVTER  510
RYG54698.1      112 LSAALSNSDVGVIITDLAATDYA---ITFVNAAFERITGYTSAEVMGRNPRFLQDPDTTPT---------YIPKMRASLSAFEPYQGTILNFRKDGHLFWNEMRISPVKGSQGDVIAWLGFISDVTAK  227
WP_281022544.1  318 LSRAVETVYAGIVITDPTSQDNP---IIYVNKGFEAITGYRRRDAIGRNPRFLQDPGADAH---------KIQALRSAIEQRQRIRCTLRNRRKNGSLFYNRMTIDPVLDEAGRVSHFIGVLHDITDI  433
```



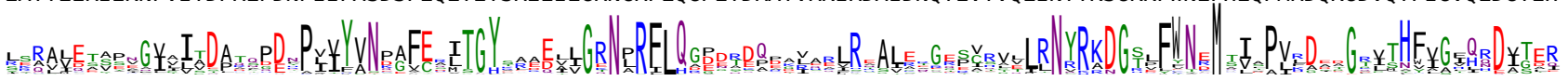
```
ME08436994.1    167 ---------------DASAD-----IVFVNPAFEKISGYRREEVIGRNPRFLQAGTAPAV---------SFAAMWATLASGKDWRGEMVNRRKDGTDYTGAMTITPVFDAAGALSAYISVQRDISRI  264
AKH98659.1      288 RSRALESAPVGILITDPDQDDNP---LIYVNDAVEDITGHSREELVGENARILQGENTDPE---------KVAEFRNAVENGESVSLELRNYRKDGTEFWNKMAIAPVRDDDGTVMNWVGFQQDVTER  403
MFB6085234.1    358 RSRALEAAPVGILITDPEQDDNP---MIYVNDAVEDLTGYKREELVGKNPRILQGENTDPD---------KVAEFRTALENEEPVTLELRNYRKDGTEFWNRMAIAPVRDDEGTVVNWVGFQQDVTER  473
WP_220580223.1  306 RTRAMDEAEVPITLADATEPDDP---IIYVNEAFESVTGYDESEILGENLRLLQGPETDPE---------TVATLREGIEAERPVTTELLNYRRDGSPFWNRMTITPIEDETGTVTHFLGFQQEVTER  421
WP_160063646.1  383 -----DEAPMGIIISNPSQDEMP---ITYVNNHFCEVTGYDEDDAIGRNPRFLQGPLTADD---------PVEKVRDAIESRTTVETDILNYRSDGTPFWNHMQIAPITDSGGDLAYFVGFQNDVTDR  493
MFN2332219.1    316 --------------SATQHDTP---VIYVNDAFCRMTGYTRDETLGQNLRFLQGPETSQN---------AVSQLRHATETCTPAQVVLLNYRKDGTRLWTNMSINPIFDEAGRCSHFVGTQQDISLE  416
MCA1772483.1     63 LQQAIEASPNGISISDARQDDTP---VVHVNKAFCQITGYNLEETRGQNLRFLQGEETSPA---------AVSVLRRAVQTQTSCEVKLLNYRKDGTLLWTRMAIGPIFNAAGQCTHFIGTQQDITAE  178
PSQ99171.1      300 MDAAMEHAEDGVLITEAHSLDEPGPKIVYANDAFCENTGYAREEVLGRNPRFLQGPETDRA---------ELDHLRAALEAEEPVRAELTNYKKDGTPFWVEMSVMPVFDAEGRCTHFTSIQRDVSER  418
MCL2092117.1     39 --------------TRAAGDNP---VVWVNDGFTTLTGYSREEALGRNLRFLQGENTDHR---------AVRQVHQALALGGTAATTLLNYRKDGMPFWNRMLIVPVCDDVGTITHHIAAHTDASLD  139
WP_321277021.1  343 ----------------GAGQR----VVFCNKGVEKLTGYSKQEVLGSNMRFLQPEGEDQS--------KVREEIRQALSIDRPSRSLLLNQHKDGHEFWNDMIITPVIDLHGQFSHYIGILHDVTDR  441
KAH7130706.1    179 LRDVVHRTSEVYFLSDPSLPDDP---IVFASQEFYNTTLYGQAYVIGKNWRFLCGPHTQAA---------AIKRIYDALNNGMEICEVLLNYRRDGSPFLNLMMMAPLMDHRGRIRYVLGRQIDITQL  294
XP_035324298.1   35 -----VDCSVSLTLCDLDLPDAP---IIYASDGFCELTGYTVPEVLGRNPRFLQNPPPEARSLITSEDRAAIRRVSRAMAQSKEIQLPITNYKKDGQPFKNIMSIVPLKLGLGDEMHNYAVGLQCEV-  153
```


b

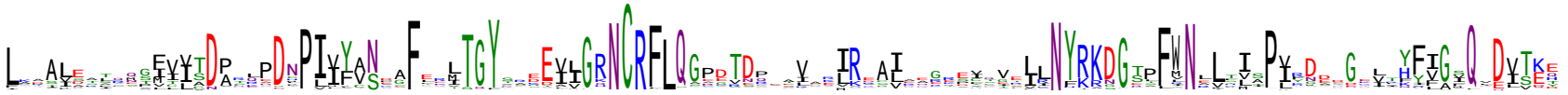


```
AsLOV2          404 LATTLERIEKNFVITDPRLPDNPIIFASDSFLQLTEYSREEILGRNCRFLQGPETDRATVRKIRDAIDNQTEVTVQLINYTKSGKKFWNLFHLQPMRDQKGDVQYFIGVQLDGTEH  519
```

logo LOVme



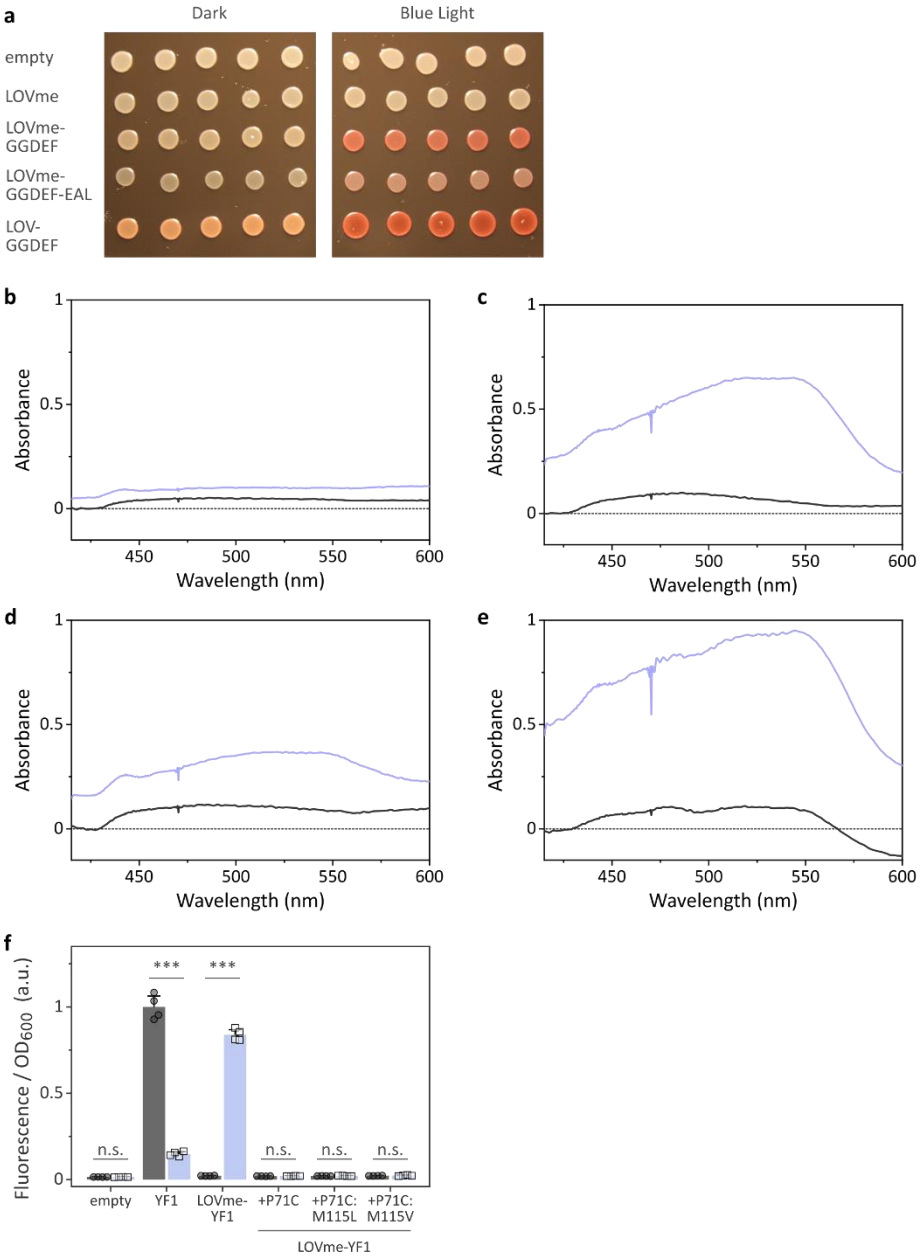
logo canonical LOV



Supplementary Figure 19

LOVme receptors in nature. **a**, Multiple sequence analyses of *Avena sativa* phototropin 1 LOV2 (*As*LOV2) and candidate LOVme receptors pinpointed in GenBank (see Suppl. Fig. 18). Grey shading and open arrows highlight residues strongly conserved across LOV receptors; red shading and black arrows mark the adduct-forming cysteine and methionine residues of canonical LOV and LOVme receptors, respectively. The circles above the alignment convey the secondary structure of *As*LOV2 (tan: α helix; blue: β strand; white: loop/unstructured). The logo below the alignment reports the sequence conservation within the LOVme group. **b**, Comparison of aggregate sequence traits in canonical LOV vs. LOVme receptors found in GenBank. The LOVme sequence logo from panel a is compared to a corresponding logo calculated for around 39,500 canonical LOV receptors. Note that the sequence logos are restricted to positions in the alignment where the *As*LOV2 reference does not display a gap. Save the positions of the adduct-forming cysteine and methionine residues, the two logos are largely similar. However, a phenylalanine (*As*LOV2 F434) within the Cα helix and the active-site glutamine (*As*LOV2 Q513) are less strictly conserved across the LOVme candidates than in regular LOV receptors.

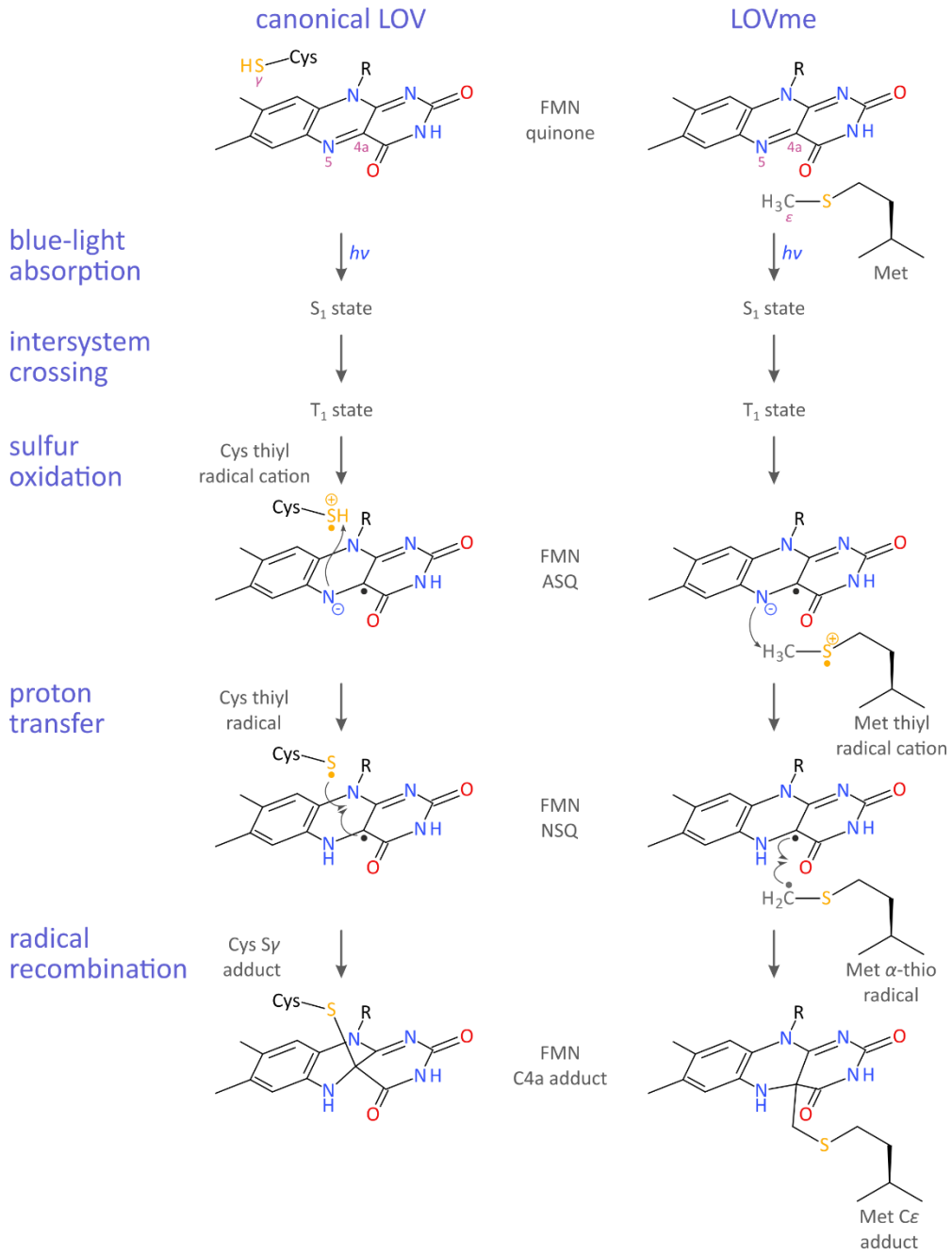
Supplementary Figure 20



Activity and light response of the naturally occurring *Rubrobacteraceae* LOVme-GGDEF-EAL receptor. **a**, As described in Fig. 5c, bacteria harboring different truncation variants of the LOVme-GGDEF-EAL receptor were cultivated under dark or blue-light conditions, followed by visualization of biofilm-formation by Congo-Red staining. Bacteria harboring an empty vector were included as a negative control. For reference, the *bona fide* LOV-GGDEF receptor *Ms*LadC was included as well [38]. **b**, Reflectance measurements of the bacteria from panel a expressing the LOVme construct. Absorption spectra were calculated with reference to the reflectance of bacteria containing the negative control. Black and blue lines denote the average absorbance signals for cultures incubated

under dark and blue-light conditions, respectively. **c**, As panel b but for the LOVme-GGDEF construct. **d**, As panel b but for the full-length LOVme-GGDEF-EAL receptor. **e**, As panel b but for *Ms*LadC. **f**, Additional variants of the LOVme-YF1 receptor were analyzed within the pDusk-*Ds*Red reporter context (see Fig. 5d for details). Symbols above the bars denote results from Welch's two-sided *t*-tests for the pairwise comparison of dark vs. light conditions (n.s. not significant, * $p < 0.05$, ** $p < 0.01$, *** $p < 0.001$).

Supplementary Figure 21



Unifying model for signal transduction in canonical LOV and LOVme blue-light receptors. Within the dark-adapted receptor, the flavin chromophore dwells in its oxidized quinone state. Absorption of UV-A and blue light excites the flavin to higher electronic singlet states that, within nanoseconds, convert to the triplet state T_1 via inter-system crossing. The photoexcited flavin is a strong oxidant capable of abstracting electrons from nearby sulfur atoms, i.e., from Sγ of cysteine and Sδ of methionine, respectively, in the case of canonical and LOVme receptors. Thereby, the flavin anionic semiquinone (ASQ) and a thiyl radical cation form. Notably, time-resolved electron paramagnetic

294 resonance spectroscopy has provided experimental evidence for the occurrence of such a radical pair
295 in canonical LOV receptors [12]. The thiyl radical cation stabilizes by proton transfer to the N5 atom of
296 the flavin which thus converts to the neutral semiquinone (NSQ) radical. Proton transfer is likely
297 aided by transient water influx into the receptor active site as previously inferred [18] and recently
298 observed [14]. In canonical LOV receptors, a neutral cysteine radical thus arises; by contrast, in LOVme
299 receptors, it is an α-thio methionyl radical. The cysteinyl/methionyl and NSQ radicals recombine into
300 a new single bond that covalently connects the flavin chromophore with the LOV protein scaffold.
301 Both the LOV and LOVme reaction series thus culminate in (meta)stable flavin N5 protonation, a
302 step necessary and sufficient [17,18] for downstream signal propagation (not shown in the figure; more
303 details in reference [18]).